Research Square

Preprints are preliminary reports that have not undergone peer review.
They should not be considered conclusive, used to inform clinical practice,
or referenced by the media as validated information.

e-Callisto Catalog of Solar Radio Bursts: Solar Cycle 24

Javier Bussons Gordo

javier.bussons@uah.es

Universidad de Alcalá

Juan José García Delgado

Universidad de Alcalá

Manuel Prieto Mateo

Universidad de Alcalá

Daniela Banyś

Institute for Solar-Terrestrial Physics DLR

Arnold O. Benz

Institute for Particle Physics and Astrophysics

Jorge Borque López-Torres

Universidad de Alcalá

Safınaz Ahmed Abdel Rahman Khaled

National Research Institute of Astronomy and Geophysics

Joaquín Martínez del Hoyo

Universidad de Alcalá

Christian Monstein

Istituto Ricerche Solari Locarno

Alexandro Rabadán Parra

Universidad de Alcalá

Vincenzo Timmel

FHNW University of Applied Sciences and Arts Northwestern Switzerland

---

Research Article

Keywords: e-Callisto, solar radio bursts, space weather, solar cycle, solar flares, coronal mass ejections

Posted Date: July 31st, 2026

DOI: https://doi.org/10.21203/rs.3.rs-10502147/v1

License: This work is licensed under a Creative Commons Attribution 4.0 International License.
Read Full License

Additional Declarations: No competing interests reported.

e-Callisto Catalog of Solar Radio Bursts: Solar Cycle 24

Javier Bussons Gordo[1] · Juan José García Delgado[1] · Manuel Prieto Mateo[1] · Daniela Banyś[2] · Arnold O. Benz[3,4] · Jorge Borque López-Torres[1] · Safinaz Ahmed Khaled[5,6] · Joaquín Martínez del Hoyo[1] · Christian Monstein[7] · Alexandro Rabadán Parra[1] · Vincenzo Timmel[4]

© **The author(s) ●●●●**

Abstract The catalog of Solar Radio Bursts detected by *e-Callisto* during Solar Cycle 24 (https://astrodoncel.uah.es/dashboard/Catalog_SC24.php) presented here comprises 5380 bursts classified by type and intensity, with more than 60 fields of information regarding contextual, geographical, morphological and physical characteristics and with dynamic spectrograms of the stations detecting each event. The catalog is enhanced with time-matching radio events from the NOAA-RSTN network, flares from NOAA-SWPC reports and CMEs from the CDAW SOHO-LASCO catalog, including their basic properties.

Keywords: *e-Callisto*, solar radio bursts, space weather, solar cycle, solar flares, coronal mass ejections

---

✉ JBG
javier.bussons@uah.es

1 Space Research Group. Universidad de Alcalá. 28805 Alcalá de Henares, Spain

2 Institute for Solar-Terrestrial Physics, German Aerospace Center (DLR), Neustrelitz, Germany

3 Institute for Particle Physics and Astrophysics, ETH Zurich, 8093, Zurich, Switzerland

4 University of Applied Sciences and Arts, Fachhochschule Nordwestschweiz, Windisch, Switzerland

5 National Research Institute for Astrophysics and Geophysics (NRIAG), Egypt

6 RAEGE Station, Santa Maria Island, Açores, Portugal

7 Istituto ricerche solari Aldo e Cele Daccò (IRSOL), Università della Svizzera italiana, Locarno, Switzerland

1. Introduction

Solar radio bursts (SRBs) are sudden enhancements of solar radio emission accompanying eruptive episodes of solar activity such as flares or Coronal Mass Ejections (CME), what makes them a valuable tool in fundamental solar physics and space weather (Wild and Smerd 1972; Klein et al. 2018). SRBs are due to beams of accelerated electrons in the keV—MeV energy range that induce rapid collective oscillations of the surrounding conductive plasma –Langmuir waves– which in turn decay into electromagnetic radio waves in a plasma-density-dependent process. Such electron beams may escape along open magnetic field lines through coronal holes and propagate in the heliosphere; they may also get trapped in stationary or moving closed frozen-field structures —the magnetic bottles mentioned in early CME models (Payne-Scott 1947 in Goss and McGee 2010; Gold 1960; Burlaga et al. 1981)— or precipitate back towards the Sun along closed magnetic lines. Therefore, SRBs bear on the understanding of the fundamental physics and geometry of the magnetic field reconfigurations lying behind these processes all the way from magnetically active regions in the photosphere to reconnection flux-ropes in the chromosphere and low corona, to solar wind heating, Solar Energetic Particle (SEP) acceleration and escape through the interplanetary medium. Furthermore, being speed-of-light signatures of the much slower shock-driving CMEs, they may be used as predictors of potentially-harmful consequences of the eventual CME and SEP interaction with the Earth's magnetosphere.

Ground-based solar radio observations in the decimetric, metric and decametric wavelength ranges, i.e. at UHF, VHF, HF frequencies, sample heliophysical processes taking place in the first two solar radii in heliocentric distance. With the advent of both single and multi-spacecraft solar observations (v.g. missions such as SOHO, STEREO, SDO, Wind, Solar Orbiter, Parker Solar Probe), similar studies extend to the Deca-hecto-kilometric domain, thereby completing the Sun-Earth journey by covering the 2—214 solar radii (1 AU) segment. Space-based coronagraph and radio spectral observations allow us to study shocks driven by coronal mass ejections. An added value of ground-based radio observations is their ability to track accelerated electrons, via SRB emission, across the full Sun-Earth path, from the Sun's photosphere (decimetric, GHz) to the Earth's vicinity (kilometric, kHz, 1 AU).

SRBs come in four major flavours or types (Pick 1986). Type I or CTM storms are the signatures of the evolution of Active Regions (AR) in the photosphere. Type II bursts signal the occurrence of shock-driving CMEs (Cairns et al. 2003). Type III bursts, along with their eventual continuation as type V events, are tracers of electron acceleration and beam broadening along open magnetic field lines (Reid and Ratcliffe 2014). Type IV SRBs are caused by electrons trapped in either moving or stationary plasma clouds Fokker 1963. Type II and type III events are particularly useful in shock and flare modelling: radio frequency is connected to plasma density and, through coronal density models, to height above the base of the corona, thus allowing the derivation of shock and beam

speeds from the frequency drift shown in radio spectrograms; beam splitting, when present, provides a good estimate of magnetic field strength; temporal correlation or delay between the radio emission and optical, UV or X-ray flares is a key diagnostic tool for the location of reconnection loops, electron injection and acceleration regions and for further electron transport —both upwards and downwards travel paths and speeds.

Therefore, both near-real-time and archival catalogs of SRB events become mandatory when dealing with space weather nowcasting and forecasting or with fundamental solar physics modelling, respectively. They are used to confirm or improve coronal density models (Newkirk 1961; Saito, Poland, and Munro 1977; Leblanc, Dulk, and Bougeret 1998) widely used in all aspects of solar physics due to the fact that most important processes involved (Langmuir waves turbulence, reconnection output, particle acceleration and scattering, etc.) depend greatly on plasma density and its fluctuations. Extensive databases of both SRBs and CMEs from ground- and space-based observatories over an entire solar cycle facilitate studies of the relationship between type II or type IV emission and their association with CMEs (Gopalswamy, Makela, and Yashiro 2019; Ndacyayisenga et al. 2021; Kumari, Morosan, and Kilpua 2021; Ma et al. 2025). These catalogs are the starting point of statistical analyses of the Sun evolution during a Solar Cycle (SC) and across different solar cycles (Mahender et al. 2020; Zhang, Wang, and Ye 2018). Early observations (Gómez-Herrero et al. 2021) and a recent catalog of Solar Energetic Electron events compiled by Solar Orbiter (Warmuth et al. 2025) support the flare-related origin of impulsive events and the asssociation of gradual events with extended structures suchs as CME-driven shocks or erupting flux ropes, which calls for a thorough cross-check with a contemporaneous (SC25) ground-based SRB catalog, currently in preparation by the e-Callisto Collaboration. Studies of the relationship between AR jets and type III bursts located near or inside coronal holes (Mulay et al. 2019), electron transport after the apex of closed magnetic loops in the descending branch (Reid and Kontar 2018; Lorfing and Reid 2023), or the scattering, trapping and emission of dense electron beams in type V bursts (Benz et al. 2024) are but a few examples underlining the importance of SRB catalogs. As they reach their maximum utility when combined with both in-situ and remote satellite observations, inter-operability with space-mission catalogs is a plus.

In Section 2 of this paper, we describe the e-Callisto Network of Solar Radio Spectrometers, its status and evolution during Solar Cycle 24, the transition from manual to automatic SRB detection and reporting, the optimization of the deARCE SRB identification model for this period, the catalog construction process and the resulting catalog fields. Results regarding e-Callisto events, matching radio events from the NOAA Radio Solar Telescope Network, matching flares and matching CMEs are given in Section 3, followed by statistical results in Section 4. Discussion of results, conclusions and future directions are provided in Section 5.

2. Description of the *e-Callisto* 2012–2019 SRB catalog

2.1. Evolution of the *e-Callisto* Network during Solar Cycle 24

e-Callisto (e-callisto.org, Benz et al. 2009, Monstein, Csillaghy, and Benz 2023), the international network of *Compound Astronomical Low-frequency Low-cost Instruments for Spectroscopy and Transportable Observatories*, –hereafter "the network"– is an International Space Weather Initiative (ISWI) instrument array deployed around the globe with the goal of understanding transient phenomena in the solar corona by monitoring radio solar emission 24 hours a day. Inspired in the framework of the International Heliophysical Year 2007 and following on the successful design of the standard CALLISTO receiver (Benz, Monstein, and Meyer 2005), the network began its deployment around the world with test stations in the Bleien Radio Observatory (Switzerland), Humain (Belgium), KASI (Korea), RCAG (Mongolia), SSRT (Siberia), Ooty and Gauribidanur in India, soon followed by MRO (Finland), Hurbanovo (Slovakia), DARO (Germany), Birr (Ireland), INPE (Brazil), Alaska (USA), Almaty (Kazakhstan) and KRIM (Crimea).

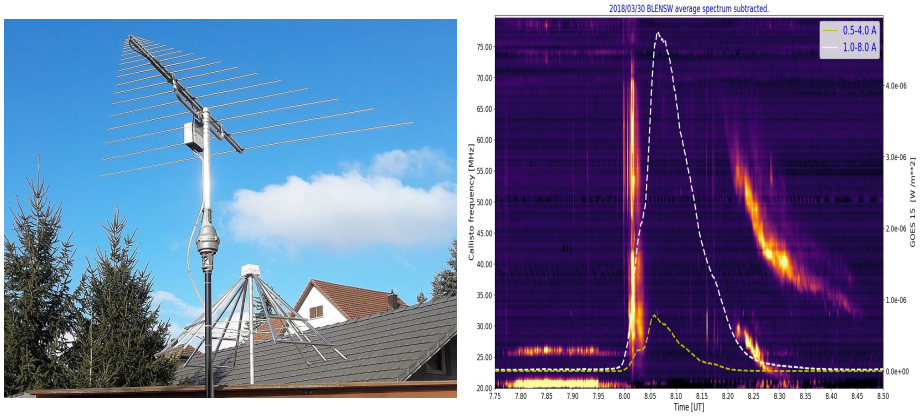


Figure 1. a) Examples of LPDA (left) and LWA (right) antennas, SWISS-MUHEN station. b) Example of spectrogram with type III (centre) and type II (right) solar radio bursts and local transient RFI (bottom left). Superimposed: X-ray flux curves of a matching flare from GOES satellite at 1–8 and 0.5–4.0 Angstrom wavelengths.

For the purposes of this paper, we consider the network fully operative since 2012: this is the reason why data from the 2009–2011 period, the first years of SC24 near solar minimum, are not included in this work. A typical *e-Callisto* station or location comprises one or more instruments —antenna plus receiver (Zucca et al. 2012; Russu et al. 2015). The CALLISTO receiver, with 0.25 seconds of time resolution at 200 channels per spectrum and an overall dynamic range larger than 50 dB, natively operates in the 45–870 MHz range but lower/higher frecuencies can be accomodated via up/down converters. As the duration of a standard observation run is 15 minutes, a typical spectrogram spans 3600

pixels in time (15*60/0.25) and 200 pixels in frequency. The most widely used antennas (Figure 2.1(a)) are the Yagi Log-Periodic Dipole Antenna (LPDA: model CLP-5130 or other) in the VHF band, the Long Wavelength Antenna (LWA, Reeve (last access: 2026/07/24); UNM (last access: 2026/07/24)) in the 20–80 MHz band and commercial L-band dipoles. However, full standardization is not possible as each host institution decides upon instrumentation and working frequency range considering their needs, resources and site conditions, including local Radio Frequency Interference (RFI), which is clearly getting worse (Prieto et al. 2020).

Figure 2 shows the historical evolution of the *e-Callisto* network. The number of locations N_{locs} grew, already in 2012, from 15 to 26, while the yearly average grew steadily from 22 in 2012 to 30 in 2014 (solar maximum) and 46 in 2019. A similar steady growth is seen in the number of different instruments N_{inst}, with yearly averages of 29 in 2012, 38 in 2014 and 62 in 2019. In the number of daily runs N_{runs}, apart from a similar trend in yearly averages (1010 runs or spectrograms per day in 2012, 1742 in 2014 and up to 3068 in 2019, i.e. more than 750 hours of observation per day across the planet), we notice a seasonal sinusoidal-like modulation inside each year, with maximum in northern summer and minimum in northern winter, due to the asymmetrical distribution of *e-Callisto* locations, clearly biased towards northern latitudes (see Figure 6(a)).

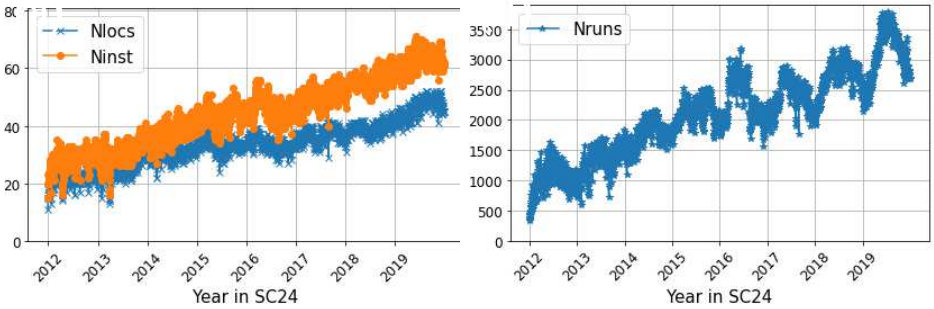


Figure 2. Evolution of the e-Callisto Network. a) Nlocs: number of stations or locations; Ninst: number of different instruments. b) Nruns: number of 15-minute-long data runs or spectrograms per day.

The effect of asymmetry in geographical longitude λ is shown in the left panels of Figure 3: the bulk of the number of hours of observation during the 8-year period is found in the $-10° < \lambda < 60°$ interval (Europe and Africa), with a secondary bump in Asia, around $\lambda = 100°$ and lower coverage on both sides of the International Date Line, $-180° < \lambda < -150°$ and $150° < \lambda < 180°$. The evolution of the geo-longitudinal distribution of stations from 2012 to 2014 to 2019 is shown in the bottom left panel: the bias remains through the period but an effort has been made to encourage the installation of new stations in lower-coverage zones. This is an undergoing effort: during Solar Cycle 25, new sites have been set in operation in areas such as New Zealand, Australia, Uzbekistan,

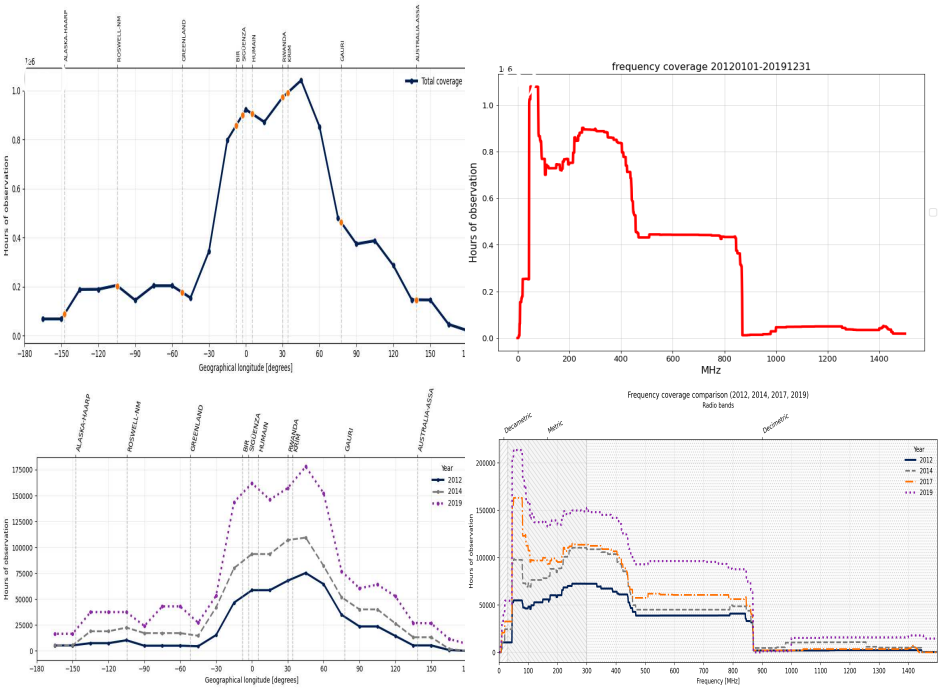


Figure 3. Left: geographical longitude coverage (orange dots indicate the position of some reference stations). Right: frequency coverage. Top panels show total coverage in 2012–19 while bottom panels show coverage evolution across the cycle.

Azores or Mexico.

Another important experimental aspect is frequency coverage. Figure 3, top right, shows a peak in the 20–80 MHz band, followed by successively smaller coverages in the 210–450 MHz, 80–210 MHz, 450–850 MHz and > 850 MHz ranges, all due again to the choices made by each host institution based on local RFI conditions and availability of resources and by the fact that most interesting SRB features detectable by ground-based instruments show up at low VHF and HF frequencies. In the yearly evolution shown in the bottom right panel, a steady increase in observing time by LWA-like detectors in the 20–80 MHz band is noticeable. This frequency band, bordering the ionospheric cutoff below which radio observations must be made from space, yields particularly interesting information about processes taking place around 2 solar radii in heliocentric distance.

2.2. Optimization of parameters for SRB detection

It is important to mention that, due to very limited manpower during the early years of the e-Callisto network (SC24) and the fact that the search for SRBs in the data had to be done manually by visual inspection of up to 3000 spectrograms a day, no official SRB reports were issued. Only with the development in 2023 of

the deep-learning-based Automated Radioburst Compilation Engine (deARCE, Bussons Gordo et al. 2023), has it been possible to address this issue, first focussing on the production of contemporary reports, available daily at the UAH AstroDoncel Data Center[1], located at La Casa del Doncel in Sigüenza (Spain), and then moving back in time to the analysis of archival data from SC24.

Since its publication, deARCE, as Convolutional Neural Network Model, has evolved from an AlexNet model run on NVIDIA/DIGITS to DenseNet121 and then ResNet18 models run on PyTorch. The transition from png to parquet files has allowed us to improve the reporting cadence from a daily to an hourly basis. Although it is currently being enhanced with SRB-classification-by-type capabilities, for the SC24 catalog it has been used strictly as SRB event detector, not classifier. It features two tunable parameters: the percent probability threshold th above which a 1-minute-long spectrogram slice is considered to host an SRB and the minimum number k of e-Callisto locations with a positive detection that we require (coincidence trigger criterion). Demanding detections in more stations (higher k) is a good way to avoid False Positives (FP) but this comes with a loss of genuine bursts (False Negatives, FN). Similarly, raising the threshold th results in fewer FPs but more FNs.

As the $th = 50,\ k = 3$ default combination currently used with SC25 data has been optimized with the present configuration of the network, which may not represent the SC24 situation, these parameters were optimized as follows. First, using as main input the total daily sunspot number (ROB-SILSO: Sunspot Index and Long-term Solar Observations[2]) and as secondary inputs the CME report from CDAW[3] and the RSTN SRB report from NOAA, 12 particularly active dates in 2014 (solar maximum) were selected, one in each month so as to avoid focusing on a particular season. Then, all the *e-Callisto* spectrograms corresponding to those dates were manually inspected by a team led by the Chief Observer (Ch. Monstein) and a master "ground-truth" burst list was produced comprising 115 events of all types. Finally, deARCE was run on the data with 16 different (th, k) combinations: $th = \{20, 40, 60, 80\}; k = \{2, 3, 4, 5\}$ and for each of them an output report was issued and compared with the master list, thus yielding the False Positive and False Negative metrics. The results are shown in Figure 4: considering our policy by which higher values of th and k are preferable in order to focus on major bursts as opposed to producing unmanageably long lists of SRBs, the best-compromise $th = 40, k = 3$ configuration was chosen for the catalog presented here.

2.3. Catalog: Fields and Entries

The automatic SRB identifier model (deARCEv3) with $th = 40,\ k = 3$ was applied to *e-Callisto* SC24 data, resulting in 6081 events. Given the often-long-

[1] https://astrodoncel.uah.es.

[2] https://www.sidc.be/SILSO/home

[3] https://cdaw.gsfc.nasa.gov/CME_list/radio/waves_type2.html.

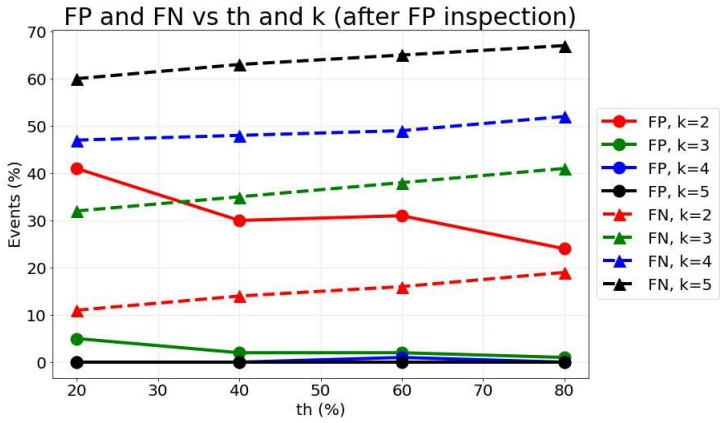


Figure 4. Optimization of model parameters: *th*: probability threshold for positive detection; *k*: minimum number of triggering stations. Metrics: FP (false positives); FN (false negatives)

duration nature of type IV events, for which deARCE was not trained, this list was enhanced with 117 type IV events (marked with `key=b`) belonging to the so-called "RSTN-only" set, i.e. those detected by RSTN but not by deARCE. Manual inspection and classification of the resulting database by a task force at UAH followed, with the goal of assigning a Type and Intensity to each burst as well as removing false positives and redundant events (typically a time interval selected by deARCE with partial overlap with a long RSTN interval: the most informative of them was kept and the other one, removed). The task of manually classifying the $\sim$ 6000 events selected by deARCE, with roughly 5 different station views each, was tough indeed, but nothing compared to what would have been required in the absence of an automatic model —checking 3000 spectrograms per day for 8 years, around 8.76 million spectrograms. In the process, 960 False Positives (15%) and 39 redundant events were removed, rendering a catalog with 5199 events. Table 1 summarizes the process with a yearly breakdown. A breakdown by type is given in Table 2.

The SC24 catalog is available at the UAH AstroDoncel Data Center: https://astrodoncel.uah.es/dashboard/Catalog_SC24.php.

Figure 5 shows a screenshot of the catalog, which is arranged in tabular format, with each row devoted to a Solar Radio Burst (or entry). Consecutive rows with the same time interval (entries marked with `key=c`) imply two or more sufficiently different types of bursts occurring during the same interval (or event). For this reason, there are 5380 entries in the catalog but just 5199 different intervals.

An explanation of the main catalog fields or columns follows (for a full explanation see the README file on the AstroDoncel web portal):

- Date: in yyyy/mm/dd format.

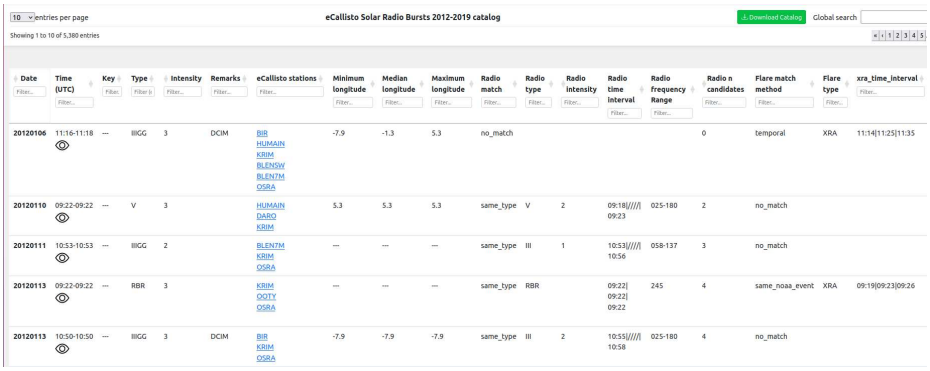


Figure 5. Screenshot of the e-Callisto SC24 Catalog

• Time interval: start and end UT times. Minimum interval is 1 minute and deARCE concatenates 1-min spectrogram slices into a single interval as long as it does not find a period of more than 3 minutes without a positive detection.

• Spectrogram icon: by clicking on the icon, it renders the full event as seen by all stations with positive detection.

• Key:

"a": event associated with or close (< 10 min) to a type II event, given the special importance of episodes surrounding type II bursts

"b": event associated with or close to a type IV event —selection triggered by RSTN-only type IV intervals at frequencies < 180 MHz, often spanning several hours. As their intensity in e-Callisto spectrograms is hard to define, we retain that of RSTN.

"c": compound event. If more than one major burst type (usually II, III, IV) appears in the same interval, a duplicate entry is made for each one. This is not done, however, when two manifestations of the same burst appear at different frequency ranges (say, a decametric type III with metric or DCIM extension, or different harmonics of the same burst).

• Type: manually assigned by the Observer On Duty (OOD). Twelve types are available: CTM (type I storm), II, III, IIIG, IIIGG, J, U, IV, V, DCIM (decimetric, in this context usually > 300 MHz), RBR (near-monochromatic bursts), Other. According to the 1988 Zürich classification: G = group of 6 to 10 bursts; GG = group of more than 10 bursts. For certain purposes, types III, IIIG, IIIGG, J, U and sometimes V are grouped together in what we call the III* family. Types IIIG, IIIGG are equivalent to NOAA's type VI.

• Intensity: manually assigned by the OOD. It gives an indication of the apparent burst intensity —averaged over all the stations— taken from the spectrogram color heat map, bearing in mind that the stations are not intercalibrated and that the measured signal also depends on the Sun's position relative to the antenna beam pattern, as not all the stations have a tracking system. When IIIG or IIIGG groups show individual bursts of different intensity, the most intense one is typically used but this is quite subjective.

• Remarks: made by the OOD, often regarding a secondary component added to the one given in the Type field (see below), interesting burst features, possible

association with other surrounding events or the real duration of an eruptive episode known by other means.

"`/r`": reverse-drift feature

"`/p`": possibly polarized event (when a station instrument with such capability shows different burst views in opposite polarizations)

"J, U or V features": when a type III-like event seems to show horizontal branch, descending branch or pole-and-flag features, respectively, but they are not clear enough to categorize them as such. The end user interested in this kind of bursts is encouraged to search for "`J`", "`U`" or "`V`" strings not only in the Type field but also in Remarks. Likewise with "J, U harmonics".

When, as opposed to the aforementioned compound event (`key=c`) category, more than one signature of similar-type bursts is seen, the main one is given as Type and the rest are included as Remarks. Typical examples are DCIM harmonics of a type III burst or J features inside a type III group. If type III activity is seen at HF frequencies, this is marked as Type=III; if, in addition, DCIM activity is seen, this is marked via Remarks = DCIM or DCIM harmonics; if only DCIM activity of the type-III kind ("legs" at > 300 MHz) is seen, then Type=DCIM. "DCIM continuum" is used when no individual vertical spikes are visible, whereas "DCIM pulsation" refers to wide-band non-drifting structures made of vertical spikes for several minutes; if longer than 10 minutes with no clear spikes, it may be a type IV.

• Stations: comma-separated list of stations with a positive detection in that time interval. Detections triggered by $k = 3$ that, after False Positive revision, have less than three stations, are kept nevertheless. By clicking on a given station, the corresponding raw FITS file is downloaded .

• Minimum, median and maximum geographical longitude: they refer to the *e-Callisto* stations detecting the event.

• Type_auto, Intensity_auto: type assigned via a feature-based machine learning model and intensity estimated using the Y-factor and SNR as proxies.

• Y-factor and Signal-to-Noise Ratio (SNR): defined, respectively, as $10 \log \frac{I_1}{I_0}$ and $10 \log \frac{I_1 - I_0}{\sigma}$ where I_0, I_1 are the average and peak noise intensities in the spectrogram, respectively, and σ is the root-mean-squared noise. For the noise estimation, the median of 5 frequency channels is used in order to avoid biases due to hot pixels. The final Y-factor and SNR values are weighted averages over all triggered stations.

• tmin, tmax, fmin, fmax: burst localization in the time-frequency domain.

• Drift rate: defined as frequency variation per unit time (work in progress).

• Results of the search for time-coincident radio events from the NOAA-RSTN network: apart from parameters returned by NOAA (burst type, intensity, time interval, frequency range) we define the `radio_match_method` (see Section 3.2), the number of matching candidates `radio_n_candidates` and the overlap between *e-Callisto* and RSTN time intervals `radio_overlap`.

• Results of the search for time-coincident flare events from the NOAA-SWPC Solar and Geophysical Events Report: besides parameters returned by NOAA (flare type: XRA/XFL/FLA, time interval, XRA class: A/B/C/M/X, integrated flux, flare location, active region, flare importance, brightness) we define the `flare_match_method` (see Section 3.3), the burst–flare time difference `xra_dt`,

the number of matching candidates `flare_n_candidates` and a summary of parameters for candidates other than the primary one `flare_other_candidates`.

• Results of the search for time-coincident CME events from the SOHO-LASCO CME list: apart from parameters returned by CDAW (CME ID, first appearance time, central/mean position angle, width, initial/linear/final speeds, speed at 20 solar radii, acceleration, mass, kinetic energy, halo type, remarks) we define the `cme_match_method` (see Section 3.4), the burst–CME time difference `cme_dt_srb`, the flare–CME time difference `cme_dt_flare`, a flag for halo type (non-halo, full or partial) `cme_halo_type`, a summary of parameters of each candidate (ID, linear speed in km/s, URL link) `cme_candidate_links` and the number of matching candidates `cme_n_candidates`.

3. Catalog Results

3.1. *e-Callisto* events

Table 1 summarizes the results of the catalog-building process. In eight years of operation, *e-Callisto* observations yield 5380 Solar Radio Bursts corresponding to 5199 different time intervals, a wealth of detections now open to the scientific community. Roughly half of them (2748) confirm detections reported by NOAA-RSTN (5-station network), thus adding views of the same episodes from other geographical longitudes and most often at complementary frequencies. Furthermore, as many as 2632, 49% of the total, are either completely new bursts (337) or events reported by both networks, but where *e-Callisto* information either differs from RSTN's (different burst type time interval) or is complementary. The yearly number of Entries follows the Solar Cycle trend, with top values (1070, 1154) in 2014–15 around solar maximum, intermediate values on both sides of it (677, 742 in 2012–13; 766, 703 in 2016–17) and lower values (34, 234) in 2018–19 —and supposedly in 2009–11 when the network was not operative—, corresponding to the cycle tails.

Table 2 is a yearly breakdown of SRBs by type. The solar cycle trend is also apparent in all burst types, with certain nuances for types CTM and IV, known to be prone to misclassification.

3.2. Cross match with RSTN SRBs

For each *e-Callisto* SRB entry we search for RSP/RBR entries in the NOAA-RSTN daily report using symmetric time windows around the SRB interval, defined as $[t_{\rm start} - \Delta t,\, t_{\rm end} + \Delta t]$, where $\Delta t = 15\,$min by default, 30 min for type II bursts, and 60 min for type IV and CTM. If several radio candidates are found, priority is given to the one with the same radio type, then to the NOAA representative in the report, then to the closest start time. In these cases, we set the `radio_match_method` flag to `same_type`. If no such same-type candidate exists, other type candidates within the time window are considered,

Table 1. Yearly breakdown of the construction of the *e-Callisto* Catalog of Solar Radio Bursts for Solar Cycle 24. During 2009–2011 the network was not fully operative. deARCE: events triggered by the automatic CNN model; b: events associated with or close to an RSTN-only type IV interval; fp+red: sum of eliminated events (false positives + redundant events); Intervals: number of different time intervals (deARCE+b-(fp+red)); Dupl: entries added due to compound (key=c) events; Entries: number of different bursts (Intervals+Dupl); eC_only: events detected by e-Callisto but not by the RSTN network; Partial: events detected by both ground-based networks where e-Callisto adds partial or complementary information (significant difference in burst type, time interval).

Year	deARCE	b	fp+red	Intervals	Dupl	Entries	eC_only	Partial
2012	623	31	12	642	35	677	28	280
2013	707	29	13	723	19	742	23	285
2014	1138	27	126	1039	31	1070	36	404
2015	1522	17	417	1122	32	1154	59	494
2016	1023	5	286	742	24	766	69	307
2017	746	8	84	670	33	703	76	387
2018	51	0	19	32	2	34	7	6
2019	271	0	42	229	5	234	39	132
Total	6081	117	999	5199	181	5380	337	2295

Table 2. *e-Callisto* SC24 bursts by type. III*+JU: sum of type III bursts (both single and in groups) along with J or U bursts. Other: DCIM, RBR. a: events associated with or close (< 10 min) to a type II event.

Year	CTM	II	III*+JU	IV	V	Other	a
2012	16	42	458+7	63	39	52	44
2013	21	65	525+5	56	29	41	35
2014	57	96	689+15	43	69	101	51
2015	50	47	883+38	46	55	35	29
2016	83	11	588+38	12	21	13	5
2017	8	27	547+44	21	30	26	22
2018	1	1	25+0	1	4	2	2
2019	2	7	204+11	2	4	4	6
Total	238	296	3919+158	244	251	274	194

again giving priority to the NOAA representative, then to the closest start time. In these cases, the assigned flag is `time_only`; otherwise, it is set to `no_match`. For this match, we define the `radio_overlap` score, which is calculated solely as a diagnostic measure of the temporal agreement between the NOAA and *e-Callisto* intervals; it is not used to select the radio match.

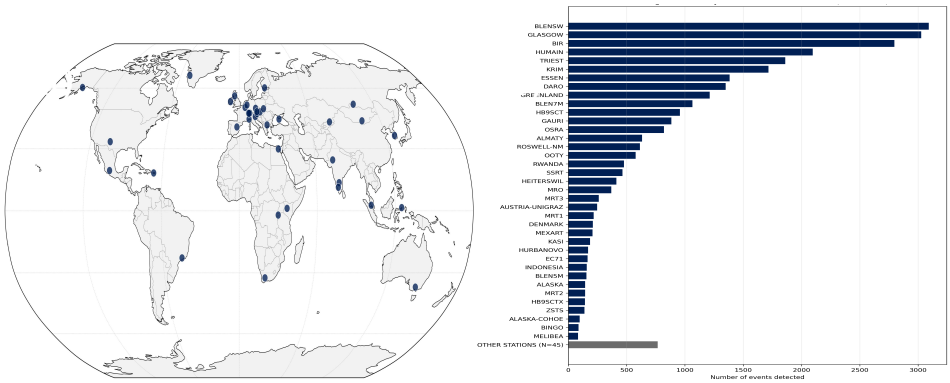


Figure 6. Left: distribution of stations around the world. Right: Ranking of stations by number of bursts detected.

3.3. Cross match with flares X-ray and Optical Flares

Once an RSTN radio match is selected, all NOAA XRA, XFL, and FLA entries sharing the same NOAA Event ID are retrieved. Entries with the same NOAA Event number are treated as different descriptions of the same physical flare rather than as separate flare candidates. Their information is preserved independently in the XRA, XFL and FLA fields. If no same-event flare exists, we apply the same symmetric time window used for the RSTN-SRB cross-match, with $\Delta t = 15\,\mathrm{min}$. This deliberately conservative margin is adopted to accommodate potential timing differences between the radio and flare detections while maintaining a simple and consistent cross-matching criterion.

3.4. Cross match with CMEs

The reference time, t_{ref}, is the flare start time if a matching flare was found; otherwise, it is the SRB start time. When the same matched flare is represented by multiple NOAA entry types, the priority order is XRA, XFL, FLA. We search for CDAW/LASCO CMEs (Yashiro et al. 2004) by first LASCO/C2 appearance, using the asymmetric time window $[t_{\mathrm{ref}} - 30\,\mathrm{min},\ t_{\mathrm{ref}} + 3\,\mathrm{h}]$, as CMEs are expected to appear after the low-corona/radio event. If several CME candidates are found, we select the one closest to the reference time and with the smallest positive delay. If no post-reference CME exists, we look for CMEs up to 30 min before the reference time and select the closest one. Negative `cme_dt_flare` or `cme_dt_srb` values identify these pre-reference cases. All physical CME-related columns describe only the selected CME. Because this association is based solely on temporal compatibility, rather than on a detailed and particular physical analysis, the selected CME cannot always be considered as an unambiguous match. We therefore retain information on all compatible candidates. The `cme_n_candidates` field gives their total number, while `cme_candidate_links` provides their identifiers, linear speeds, and links to the corresponding entries in the original CDAW/LASCO catalog. This allows users to access the source

data easily, perform a more detailed physical analysis of each event and report potential mismatches.

4. Statistics

Let us draw some statistics about the following parameters:

• Type. The fraction of bursts by type is shown in Figure 7. The vast majority (76%) of solar radio bursts detected belong to the type-III kind (III, IIIG, IIIGG, J, U), the rest being shared in similar amounts among types II (5.5%), IV (4.5%), V (4.7%), CTM (4.4%) and DCIM(4.7%), with marginal amounts of U- and RBR-bursts. The yearly trend in Figure 8 resembles that of the solar cycle, with a bump near solar maximum (2014–15), shoulders on both sides (2012–13 and 2016–17) and a tail (2018–19). Types II, CTM and V peak in 2014; the broad type-III category (by far the most numerous, note the scale on the right vertical axis) peaks in 2015, and CTM bursts peak in 2016. Higher numbers of type-IV bursts in 2012 and 2013 may indicate misclassification.

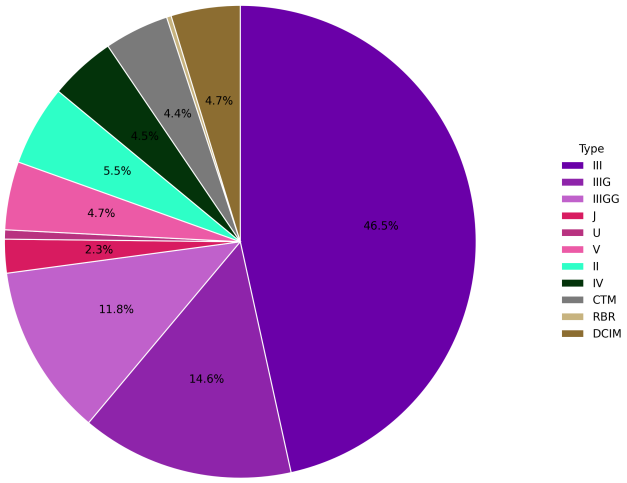


Figure 7. SRB percentages by type.

• Duration. In the absence of an accurate automatic SRB boxing mechanism to find the exact start/end times, burst duration is given by the deARCE output time interval in 1-minute units —concatenation of 1-minute intervals with positive detection. Minimum time is, thus, 1 minute. Individual type III bursts have the shortest duration (median of 1 min), which grows as the groups get more populated (2 minutes for IIIG and 5 minutes for IIIGG). Type V bursts are a bit longer than type IIIs (2 minute median) as expected from the so-called "flag" of non-drifting emission which follows the initial type III emission ("pole"). DCIM and RBR bursts usually last for less than one minute, most of them being strongly connected to individual type III bursts (the isolated "legs" or "heads", respectively). Type II bursts show median duration of 9 minutes,

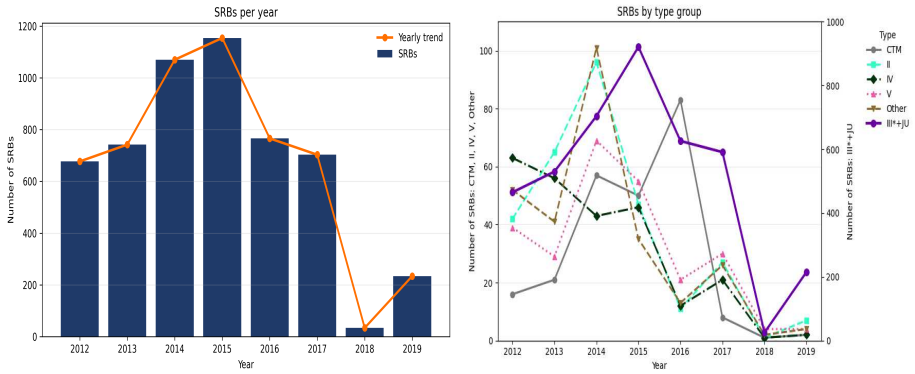


Figure 8. SRBs per year: a) overall b) by burst type (notice the different scale in the right y-axis for the type-III family).

consistent with common knowledge, with a distribution that dies out beyond 30 minutes. The type IV distribution, with a median of 24 minutes, is long-lived as expected, the upper limit of 1440 minutes (24 hours) being imposed by the date change. This category is, along with CTM (median of 2 minutes but sometimes reaching one-hour duration or more), the most vulnerable to uncertainties in time start/end definition and to misclassification.

• Intensity (manually assigned by the Observer On Duty), see Figure 11. Intense (force-3) bursts represent 45% of the total; intermediate bursts, 37%, and weak (force-1) bursts, the remaining 18%. No clear trend is seen in the yearly evolution. An automatic, more robust estimation of the intensity, currently under study by our team, is expected to give more objective information in the future.

• UT Time-of-the-day occurrence. Since solar bursts are expected to occur evenly distributed at any time of the day, the Gaussian-like distribution shown in Figure 12(a) seems to be caused by the uneven collection area of the *e-Callisto* array, heavily biased towards "European-like" longitudes as seen in Figure 3.

• Monthly evolution of SRB counts. Two overlapping trends are noticed in Figure 12(b): the intra-year monthly variability shown by the blue-bar histogram, which reflects the same latitude bias causing the seasonal undulations in N_{runs} mentioned in Section 2.1 (Figure 2(b)); and the overall solar-cycle-like trend, with stronger clustering around the 2014–15 maximum. The orange line combines both trends.

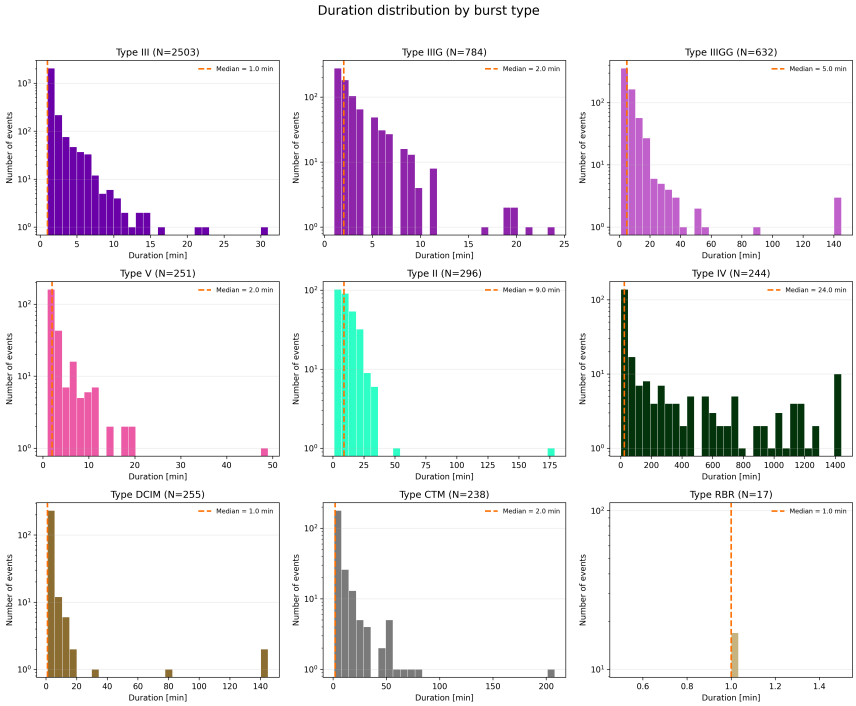


Figure 9. SRB duration by type.

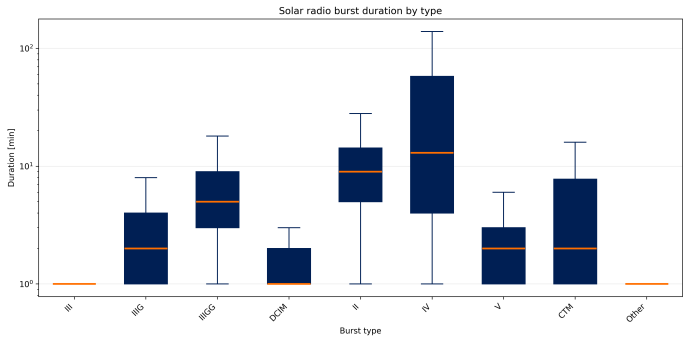


Figure 10. Boxplot of SRB duration (logarithmic) by type. Orange line: median. Blue box: Q1 to Q3 percentiles. Blue whiskers from minimum to maximum values.

A brief and preliminary insight into the cross-matching results is provided below. These statistics must be considered solely as a first descriptive assessment of the associations obtained with the temporal criteria described in Section 3, not as definitive evidence of physically-related phenomena.

• SRB e-Callisto/RSTN cross-match. RSTN radio counterparts were found for 5044 of the 5380 SRBs: 2750 (51.1%) were same-type matches, while 2294 (42.6%) were associated through temporal compatibility. The remaining 336 events (6.3%) had no RSTN counterpart. Considering all different burst types, we

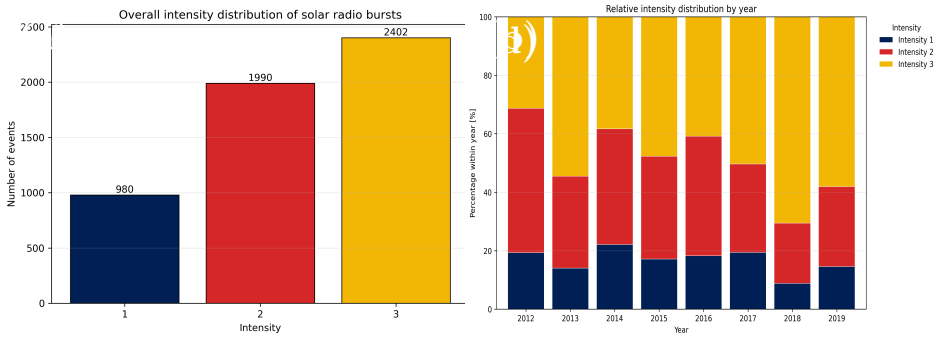


Figure 11. Intensity distributions.

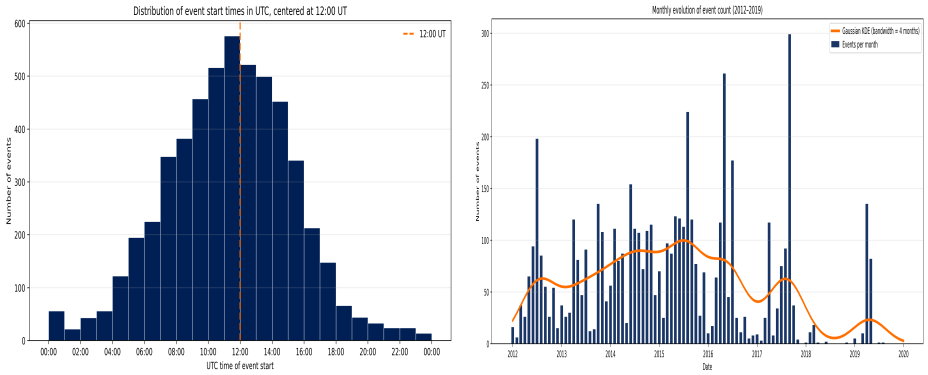


Figure 12. a) Time of the day of SRB occurrence (UT). b) Monthly evolution of SRB count and Kernel Density Estimation fit with KDE bandwidth of four months.

found the highest same-type agreement for type II (94.3%) and type IV (79.5%), followed by CTM (66.8%) and type V bursts (64.5%). For the dominant type III, 49.8% were same-type matches, while 43.6% were temporal fallback associations.

• SRB-flare associations. A matching NOAA flare was identified for 2680 SRBs (49.8%): 1956 (36.4%) share the same NOAA Event ID, while 724 (13.5%) were matched through temporal compatibility. The largest association fractions are found for type II (89.2%) and type IV (87.7%), with type III having an association rate of 44.0%. Regarding the 3919 type III* bursts in our catalog, 1723 (44.0%) were associated with a flare, and 1179 had a known GOES class. Among these, C-class flares were the most frequent (57.9%), followed by B-class (28.2%), M-class (12.0%), and X-class flares (2.0%).

• SRB-CME associations. A CDAW/LASCO CME counterpart was found for 3446 SRBs (64.1%), corresponding to 1660 unique CMEs. The largest association fraction was found for type II (94.3%), followed by type IV (83.6%) and type V (76.5%). The particularly high fraction for type II bursts is consistent with the expected connection between type II radio emission and CME-driven shocks.

A more detailed analysis of these associations between SRBs, flares and CMEs, including their physical and temporal relations, will be presented in a dedicated follow-up study.

5. Discussion, Conclusions and Future Directions

Having described in detail the catalog contents, we now discuss its value and draw some conclusions before mentioning some work in progress and future directions. To the best of our knowledge, no such comprehensive catalog of SRBs for Solar Cycle 24 has been published before.

The deployment of the *e-Callisto* Array around the world has been a major undertaking. With first discussions in 2007 and without a supra-national authority or funding entity to support and coordinate the effort, having 22 stations by 2012 ready to cover the best part of Solar Cycle 24 was already a successful start, steadily improved year after year: 30 stations in 2014 and 46 by the end of the cycle. Over 35 different countries have been part of *e-Callisto* in SC24, during which around 1.5 million hours of radio observation have been accumulated. In this paper, the substance of such an underexploited wealth of data has been extracted in the form of a comprehensive Solar Radio Burst Catalog. Inter-operability with catalogs from other ground-based experiments and space missions has been implemented in some of its fields via direct cross-matching results or links to external events and is extendable to other present and future catalogs thanks to its user-friendly matrix-like (csv) format.

The catalog exploits the strengths of the *e-Callisto* Network, namely its broad and dense geographic coverage ($\sim$ 40 stations as opposed to RSTN's 5, for instance) and its geo-redundancy, with multiple stations in similar time zones providing overlapping views of the same process and allowing the application of the tunable coincidence criterion: requiring that a minimum of 3 separate stations ($k = 3$) issue a positive detection is a strong filter against local-RFI-induced signals and False Positives caused by other natural phenomena such as lightning, reflections on water or ground, etc. It also exploits the multi-frequency nature of the network, with strong coverage of complementary HF, VHF and UHF bands, peaking in the 20–80 MHz range, followed by the 210–450 MHz, 80–210 MHz and 450–850 MHz ranges, and lighter coverage at $>$ 850 MHz.

The 5380 SRBs of the catalog include, each, text parameters with contextual, physical and morphological parameters as well as raw and processed spectrograms for all the involved stations, cross-matches with other catalogs and links to certain matching results, a mine of information now open to the scientific community. Regarding the *e-Callisto*/RSTN cross-match, roughly half of the bursts are either new bursts or events reported by both networks but where *e-Callisto* information either differs from RSTN's or is complementary. *e-Callisto* data have so far been used in around 80 papers; with this catalog, we hope to maintain its usefulness and increase its impact on the scientific community.

Work in progress includes real-time construction of the SC25 catalog and expansion of both catalogs with automatic estimation of physically meaningful and quantifiable parameters, essential to advance the study of SRBs. We focus on SRB localization in the time-frequency domain (boxing), type and intensity classification, and drift-rate calculation, which in turn allows for derivation of shock or flare speeds, acceleration, or magnetic field strength. We also combine morphological and intensity-based criteria with post-processing steps to better discriminate SRBs from RFI. Ultimately, these approaches improve the characterization of solar radio activity and its potential implications for space weather monitoring.

Future work should include: i) Physics exploitation of the catalog, focusing on episodes of strong activity but also by finding clustering of not-so-strong but persistent activity. ii) Cross-matching with Solar Orbiter's Co-SEE-Cat catalog of Solar Energetic Electron events in order to further check the purported flare-related origin of impulsive type-III events or the association of gradual type-II events with extended structures such as CME-driven shocks or erupting flux ropes. iii) Geophysical studies of Solar Radio Burst / Flare correlations with geomagnetic storms and other manifestations of induced terrestrial currents and magnetic activity measured by magnetometers and other terrestrial indices, beginning with X- and M-class X-ray flares. We are moving towards a New Generation *e-Callisto* Network by exploring and testing new types of receivers (SDR), antennas (leaky-wave Gómez-Tornero et al. 2025 and other) and data management systems along with a clever expansion of the network to new low-RFI sites in key geographical areas.

APPEAL TO END USERS FOR SUGGESTIONS: if you find or know about missing, misclassified or mismatched events, or if you have any suggestions which may improve the usability of the catalog, please send your comments to astrodoncel@uah.es

Acknowledgements This research work has been funded by the Junta de Comunidades de Castilla–La Mancha and the European Union through the CELESTINA-SPARC project (SPace-weather Awareness ad Research Center, code SBPLY/23/180225/000071).

We thank the FachHochschule NordWestschweiz and Universidad de Alcalá for hosting the e-Callisto Mirror Data Centers.

JBG and MPM thank Patricia Rodrigo for careful maintenance of the Astrodoncel Data Center at La Casa del Doncel in Sigüenza and Abel Moreno from Peralejos de las Truchas for technical assistance.

Credit is given here to past and present staff members in each e-Callisto station for commissioning and maintenance of their instruments and for uploading their data to the network data centers.

Upon retirement of Ing. Monstein, the rest of the authors pay him homage for his immense effort in the design, deployment, maintenance and exploitation of the e-Callisto Network, and for his extraordinary production: daily burst lists for years, technical reports, hardware (including over 200 CALLISTO receivers), software (web page and analysis scripts), travel to tenths of countries, training, capacity building and promotion of science.

Disclosure of Potential Conflicts of Interest The author declares that there are no conflicts of interest.

Data and Software Availability Statement The datasets analysed and generated during the current study are available from the corresponding author on reasonable request.

Author Contribution J. Bussons Gordo, M. Prieto Mateo, J.J. García Delgado, A. Rabadán Parra and J. Borque López-Torres devised the method, performed the analysis, maintained the Astrodoncel data server and portal and drafted the manuscript with input from all authors.

Ch. Monstein, besides being responsible for the deployment and maintenance of the e-Callisto network worldwide and for its data management plan, performed expert visual inspection of solar spectrograms and supervised the method and findings of this work.

A.O. Benz supervised the construction of the catalog.

S.A. Khaled performed optimization and statistical analysis for the production of burst lists and interpreted the results.

J. Martínez del Hoyo performed modelling of the e-Callisto network and optimization of the data analysis pipeline.

V. Timmel and D. Banyś advised on technical details and supervised the catalog construction.

Funding Open Access funding provided thanks to the CRUE-CSIC agreement with Springer Nature. This research work has been funded by the Junta de Comunidades de Castilla–La Mancha (JCCM) and the European Union through the CELESTINA-SPARC project (SPaceweather Awareness and Research Center, code SBPLY/23/180225/000071). JBLT is funded by the INVESTIGO-JCCM (call code 03-UAH-INV-JCCM-25).

References

Benz, A.O., Monstein, C., Meyer, H.: 2005, Callisto – A New Concept for Solar Radio Spectrometers. *Sol. Phys.* **226**, 143. DOI.

Benz, A.O., Monstein, C., Meyer, H., Manoharan, P.K., Ramesh, R., Altyntsev, A., Lara, A., Paez, J., Cho, K.-S.: 2009, A World-Wide Net of Solar Radio Spectrometers: e-CALLISTO. *Earth, Moon, Planets* **104**, 277. DOI.

Benz, A.O., Huber, C., Monstein, C., Timmel, V.: 2024, Observation of an Extraordinary Type V Solar Radio Burst: Nonlinear Evolution of the Electron Two-Stream Instability. *Solar Physics* **299/10**, 146. DOI.

Burlaga, L., Sittler, E., Mariani, F., Schwenn, R.: 1981, Magnetic loop behind an interplanetary shock: Voyager, Helios, and IMP 8 observations. *Journal of Geophysical Research: Space Physics* **86**, 6673. DOI.

Bussons Gordo, J., Fernández Ruiz, M., Prieto Mateo, M., Alvarado Díaz, J., Chávez de la O, F., Hidalgo, J.I., Monstein, C.: 2023, Automatic Burst Detection in Solar Radio Spectrograms Using Deep Learning: deARCE Method. *Solar Phys.* **298**, 82. DOI.

Cairns, I.H., Knock, S.A., Robinson, P.A., Kuncic, Z.: 2003, Type II Solar Radio Bursts: Theory and Space Weather Implications. *Space Sci. Rev.* **107**, 27. DOI.

Fokker, A.D.: 1963, Type IV solar radio emission. *Space Science Reviews* **2**, 70. URL.

Gold, T.: 1960, Energetic particle fluxes in the solar system and near the earth. *Astrophys. J., Suppl.* **4**, 406. URL.

Gómez-Herrero, R., Pacheco, D., Kollhoff, A., Espinosa Lara, F., et. al.: 2021, First near-relativistic solar electron events observed by EPD onboard Solar Orbiter. *A&A* **656**, L3. DOI.

Gopalswamy, N., Makela, P., Yashiro, S.: 2019, A Catalog of Type II radio bursts observed by Wind/WAVES and their Statistical Properties. *Sun and Geosphere* **14/2**, 111. DOI.

Goss, W.M., McGee, R.X. (eds.): 2010, *Payne-Scott at Dover Heights 1945–1947: Discovery of Type I, II and III Solar Bursts and the Introduction of Fourier Synthesis in Astronomy*, Springer Berlin Heidelberg, Berlin, Heidelberg, 81. ISBN 978-3-642-03141-0. DOI.

Gómez-Tornero, J.L., Rabadán Parra, A., Gil Martínez, A., Cañete Rebenaque, D., Bussons Gordo, J., C., M., Prieto Mateo, M.: 2025, Frequency-Scanning Waveguide Antenna for Solar Radio Bursts Detection in the UHF Band. *IEEE Open Journal of Antennas and Propagation* **6/5**, 1535. DOI.

Klein, K.-L., Salas Matamoros, C., Zucca, P., : 2018, Solar radio bursts as a tool for space weather forecasting. *Comp. Rend. Phys.* **19**, 36. DOI.

Kumari, A., Morosan, D.E., Kilpua, E.K.J.: 2021, On the Occurrence of Type IV Solar Radio Bursts in Solar Cycle 24 and Their Association with Coronal Mass Ejections. *Astrophysical Journal* **906**, 79. DOI.

Leblanc, Y., Dulk, G.A., Bougeret, J.-L.: 1998, Tracing the Electron Density from the Corona to 1 au . *Solar Physics* **183**, 165. DOI.

Lorfing, C.Y., Reid, H.A.S.: 2023, Solar Electron Beam Velocities That Grow Langmuir Waves in the Inner Heliosphere. *Solar Physics* **298/4**, A52. DOI.

Ma, B., Ling, C., Wu, D., Ning, Z., Pulupa, M., Bale, S.D.: 2025, Type IV-like Solar Radio Burst Consisting of a Series of Short-time Bursts Observed by PSP. *Astrophysical Journal* **979**, 22. DOI.

Mahender, A., Sasikumar Raja, K., Ramesh, R., Panditi, V., Monstein, C., Ganji, Y.: 2020, A Statistical Study of Low-Frequency Solar Radio Type III Bursts. *Solar Physics* **295**, 153. DOI.

Monstein, C., Csillaghy, A., Benz, A.O.: 2023, e-Callisto data: Quicklook Solar Spectrogram Plots [Data Set]. *International Space Weather Initiative (ISWI)*. DOI.

Mulay, S.M., Sharma, R., Valori, G., Vásquez, A.M., Del Zanna, G., Mason, H., Oberoi, D.: 2019, Study of the spatial association between an active region jet and a nonthermal type III radio burst. *Astronomy and Astrophysics* **632**, A108. DOI.

Ndacyayisenga, T., Umuhire, A.C., Uwamahoro, J., Monstein, C.: 2021, Space weather study through analysis of solar radio bursts detected by a single-station CALLISTO spectrometer. *Annales Geophysicae (EGU)* **39**, 945. DOI.

Newkirk, G.J.: 1961, The Solar Corona in Active Regions and the Thermal Origin of the Slowly Varying Component of Solar Radio Radiation. *Astrophysical Journal* **133**, 983. DOI.

Pick, M.: 1986, Observations of radio continua and terminology. *Solar Physics* **104**, 19. DOI.

Prieto, M., Bussons, J., Rodríguez-Pacheco, J., Martínez, A., Sánchez, S., Russu, A., Monstein, C., Fernández, R.: 2020, Increase in Interference Levels in the 45 – 870 MHz Band at the Spanish e-CALLISTO Sites over the Years 2012 and 2019. *Solar Phys.* **295**, 11. DOI.

Reeve, W.: (last access: 2026/07/24), Long Wavelength Array Active Crossed-Dipole Antenna. URL.

Reid, H.A.S., Kontar, E.P.: 2018, Solar type III radio burst time characteristics at LOFAR frequencies and the implications for electron beam transport. *Astronomy and Astrophysics* **614**, A69. DOI.

Reid, H.A.S., Ratcliffe, H.: 2014, A review of solar type III radio bursts. *Res. Astron. Astrophys.* **14**, 773. DOI.

Russu, A., Gómez-Herrero, R., Prieto, M., Monstein, C., Ivanov, H., Rodríguez-Pacheco, J., Blanco, J.J.: 2015, A year of operation of Melibea e-Callisto Solar Radio Telescope. *Journal of Physics: Conference Series* **632**, 012078. DOI.

Saito, K., Poland, A.I., Munro, R.H.: 1977, A study of the background corona near solar minimum. *Solar Physics* **55**, 121. DOI.

UNM: (last access: 2026/07/24), The Long Wavelength Array in New Mexico. URL.

Warmuth, A., Sculler, F., Gómez-Herrero, R., Cernuda, I., Rodríguez-Pacheco, J.: 2025, CoSEE-Cat: A Comprehensive Solar Energetic Electron event Catalogue obtained from combined in situ and remote-sensing observations from Solar Orbiter. Catalogue description and first statistical results. *Astronomy and Astrophysics* **701**, A20. DOI.

Wild, J.P., Smerd, S.F.: 1972, Radio Bursts from the Solar Corona. *Annu. Rev. Astron. Astr.* **10**, 159. DOI.

Yashiro, S., Gopalswamy, N., Michalek, G., St. Cyr, O.C., Plunkett, S.P., Rich, N.B., Howard, R.A.: 2004, A catalog of white light coronal mass ejections observed by the SOHO spacecraft. *Journal of Geophysical Research: Space Physics* **109 A7**. DOI.

Zhang, P., Wang, C.B., Ye, L.: 2018, A type III radio burst automatic analysis system and statistic results for a half solar cycle with the Nancay Decameter Array data. *Astronomy and Astrophysics* **618**, A165. DOI.

Zucca, P., Carley, E.P., McCauley, J., Gallagher, P.T., Monstein, C., McAteer, R.T.J.: 2012, Observations of Low Frequency Solar Radio Bursts from the Rosse Solar-Terrestrial Observatory. *Solar Physics* **280**, 591. DOI.